

Modelling and parameter estimation of breakthrough curves for amine-modified activated carbons under pre-combustion carbon capture conditions

Azpiri, Rebeca; Soares Dos Santos, Douglas; Ingram, Andy; Wood, Joe

DOI:
[10.1016/j.fuel.2019.05.095](https://doi.org/10.1016/j.fuel.2019.05.095)

License:
Creative Commons: Attribution-NonCommercial-NoDerivs (CC BY-NC-ND)

Document Version
Peer reviewed version

Citation for published version (Harvard):
Azpiri, R, Soares Dos Santos, D, Ingram, A & Wood, J 2019, 'Modelling and parameter estimation of breakthrough curves for amine-modified activated carbons under pre-combustion carbon capture conditions', *Fuel*, vol. 253, pp. 1130-1139. <https://doi.org/10.1016/j.fuel.2019.05.095>

[Link to publication on Research at Birmingham portal](#)

Publisher Rights Statement:
Checked for eligibility: 31/05/2019
<https://doi.org/10.1016/j.fuel.2019.05.095>

General rights

Unless a licence is specified above, all rights (including copyright and moral rights) in this document are retained by the authors and/or the copyright holders. The express permission of the copyright holder must be obtained for any use of this material other than for purposes permitted by law.

- Users may freely distribute the URL that is used to identify this publication.
- Users may download and/or print one copy of the publication from the University of Birmingham research portal for the purpose of private study or non-commercial research.
- User may use extracts from the document in line with the concept of 'fair dealing' under the Copyright, Designs and Patents Act 1988 (?)
- Users may not further distribute the material nor use it for the purposes of commercial gain.

Where a licence is displayed above, please note the terms and conditions of the licence govern your use of this document.

When citing, please reference the published version.

Take down policy

While the University of Birmingham exercises care and attention in making items available there are rare occasions when an item has been uploaded in error or has been deemed to be commercially or otherwise sensitive.

If you believe that this is the case for this document, please contact UBIRA@lists.bham.ac.uk providing details and we will remove access to the work immediately and investigate.

1 Modelling and Parameter Estimation of
2 Breakthrough Curves for Amine-modified
3 Activated Carbons under Pre-Combustion Carbon
4 Capture Conditions

5 *Rebeca A. Azpiri Solares[§], Douglas Soares dos Santos[§], Andrew Ingram and Joseph Wood**

6 School of Chemical Engineering, University of Birmingham, Edgbaston, Birmingham B15 2TT,
7 United Kingdom

8 *Corresponding author.

9 [§]Rebeca A. Azpiri Solares carried out the process simulation work and Douglas Soares dos Santos
10 carried out the experimental work. Equally weighted contributions are attributed to their work
11 towards this article.

12 E- mail address: J.Wood@bham.ac.uk.

13 ABSTRACT: Pressure Swing Adsorption (PSA) demonstrates high potential for capturing pre-
14 combustion carbon dioxide in Integrated Gasification Combined Cycle (IGCC) power plants,
15 due to a binary mixture of hydrogen and carbon dioxide entering the separation process. In this
16 work, a seven-step PSA model was developed and compared to adsorption experiments under
17 PSA conditions (25 bar and ambient temperatures) performed with tetraethylenepentamine
18 (TEPA) and a novel blend of monoethanolamine-monomethylethanolamine (MEA-MDEA)

19 modified activated carbons, using nitrogen and carbon dioxide mixtures. The MEA-MDEA
 20 modified activated carbon showed promising results for pre-combustion PSA processes, due
 21 to their high carbon dioxide adsorption capacity and delayed break-point of about 200 s
 22 compared to the unmodified activated carbons. A sensitivity analysis carried out for the
 23 adsorbent parameters in a seven-step PSA process showed that high mass transfer coefficient
 24 values yielded to highly purified products, specifically for the light product stream (99.4%). A
 25 sensitivity analysis of the process variables showed that purity values of the heavy stream
 26 (carbon dioxide) were over 90% when the purge pressure was reduced to 0.5 bar and the carbon
 27 dioxide feed fraction increased to 60%.

28 **KEYWORDS:** CCS; Pressure Swing Adsorption; Pre-combustion; Activated carbon;
 29 Monoethanolamine.

Nomenclature

C_i	Concentration of i component in the gas phase (mol/m ³)
Q_i	Sorbent loading of i component (mol/kg)
e	Gas phase density (kg/m ³)
e_s	Sorbent density (kg/m ³)
e_w	Bed wall density (kg/m ³)
\mathcal{E}_b	Bed void fraction
\mathcal{E}_p	Particle void fraction
\mathcal{E}_t	Total void fraction
v	Gas velocity (m/s)
R	Ideal gas constant (J/mol. K)
t	Time (s)
T	Temperature (K)
T_w	Wall temperature (K)

P	Pressure (Pa)
λ	Axial heat dispersion coefficient (W/ m. K)
ΔH_i^{ads}	Heat of adsorption of i component (kJ/mol)
C_{pg}^i	Specific heat of i component in the gas phase (kJ/mol. K)
C_{ps}	Specific heat of the sorbent (kJ/kg. K)
C_{pw}	Specific heat of the wall (kJ/kg. K)
h_i	Effective heat transfer coefficient (kW/m ² . K)
μ_g	Viscosity of the gas phase (Pa. s)
d_p	Particle diameter (m)
M_w^i	Molecular weight of i component (kg/mol)
b	Langmuir isotherm constant (1/Pa)
K_i	Effective mass transfer coefficient for i component (1/s)
Q_i^*	Sorbent loading for i component in equilibrium (mol/kg)
q_m	Maximum sorbent loading (mol/kg)
D_{AB}	Diffusion coefficient (m ² /s)
D_x	Dispersion coefficient (m ² /s)
L	Bed height (m)
L_w	Bed wall thickness (m)
m_{ads}	Mass of adsorbent in the bed (g)
F_i	Molar flowrate of i component (mol/s)
V_b	Fixed-bed reactor volume (m ³)

30 **1. Introduction**

31 Reduction of carbon dioxide (CO₂) emissions from power plants is essential to prevent global
32 warming and climate change in future generations. The Intergovernmental Panel on Climate
33 Change (IPCC) has indicated that climate scenarios will find it very difficult to achieve the 2°C
34 target without CCS, since the cost of reaching the 2°C target will be 138% higher if carbon

35 capture is not included as a mitigation option [1,2]. It is a fact that nowadays coal is still one
36 of the main energy resources for electricity production, together with natural gas [3].

37 Power plants fired by these fuels are one of the major sources of carbon dioxide emissions.
38 In this scenario, further research on carbon capture and storage must be undertaken in order to
39 apply the technology on a large scale. Lack of financial support from governments and
40 expensive CCS technologies that are not practical in industry are major issues when
41 implementing the technology [4–6].

42 On the one hand, carbon capture processes related to absorption are the most mature
43 technology, and the first industrial carbon capture projects have been retrofitted in coal-fired
44 power plants in Canada and the USA using solvent based absorption. This technology is easy
45 to retrofit compared to other existing capture processes [7–9]. On the other hand, energy-
46 intensive absorbent regeneration and solvent chemical properties that cause corrosion of the
47 equipment and toxic products are the main disadvantages noted by most of the authors [10–
48 13].

49 Adsorption processes applied to carbon capture have recently gained attention in research
50 areas. High energy efficiency is one of the main advantages of the technology compared to
51 processes using solvents, due to the ease of regeneration and not heating up large volumes of
52 water during the recovery of the capture material [14].

53 Specifically, pre-combustion carbon capture applied to Integrated Gasification Combined
54 Cycle (IGCC) power plants would use feed conditions with high pressures and ambient
55 temperatures, which could considerably reduce the energy penalty of the capture process.
56 Additionally, carbon dioxide concentrations in the fuel gas would be of around 30–50%,
57 whereas in post-combustion the concentration of CO₂ is of around 10-15%. A binary gas
58 mixture of hydrogen and carbon dioxide would enter the capture process in these plants,

59 coming from a water gas shift unit [15]. This would increase the degree of success of the
60 separation process.

61 The main pilot-scale projects developed in the field of pre-combustion carbon capture
62 applied to IGCC plants use physical absorption [16]. Pressure swing adsorption (PSA) applied
63 to these plants would improve the performance of the capture process since the process gas is
64 typically above 20 bar and PSA has been successfully implemented for hydrogen purification.
65 The key challenge for pre-combustion PSA is to develop a process step which efficiently
66 concentrates the carbon dioxide product [17].

67 For PSA to be successfully applied to IGCC power plants, both the material and engineering
68 factors must be considered [18]. In terms of the process materials, activated carbon (ACs)
69 adsorbents have been shown to be ideal candidates for the adsorption of carbon dioxide via
70 PSA, due to their structural stability, their relatively cheap price compared to that of other
71 adsorbents, and their high capacity and selectivity for carbon dioxide when the process operates
72 under PSA conditions (high pressures and ambient temperatures) [19–21]. The fact that
73 carbonaceous materials have high saturation capacities make them the most suitable adsorbents
74 for pre-combustion carbon capture using PSA [17].

75 Amine-modified activated carbons have been shown to be a promising material for carbon
76 dioxide capture, due to the chemical interaction between the nitrogen-enriched basic surface
77 and the acidity of CO₂. These materials show high selectivity for the adsorption of carbon
78 dioxide but further studies are required on the adsorption/desorption kinetics of these activated
79 carbons [17].

80 Most of the research carried out with amine-modified activated carbons focused on post-
81 combustion capture for temperatures between 30 and 60°C and ambient pressures of 1 bar [22–
82 24]. These adsorbents could potentially be more efficient in pre-combustion capture. One of

83 the main challenges of post-combustion capture would be to implement an adsorption capture
84 system that can treat high flowrates of carbon dioxide at atmospheric pressures, temperatures
85 of around 75°C, low carbon dioxide partial pressures, significant oxygen partial pressures and
86 the presence of sulphur and nitrogen monoxides [7,15].

87 Some authors studied the adsorption behavior of chemical impregnated activated carbons for
88 pre-combustion carbon dioxide capture. Zhu et al. [24] showed that the studied nitrogen
89 enriched activated carbons demonstrated high uptake of CO₂ (9.3 wt%) at 0.15 bar and 25°C,
90 due to their microporous surface and the nitrogen groups. However, previous studies did not
91 show the effect that the synthesized activated carbons' surface and mass transfer properties
92 could have on the breakthrough curves and on the overall purity of the products for pre-
93 combustion binary gas mixtures.

94 Development of a PSA model that simulates the performance of the adsorbent in a fixed-bed
95 reactor could help to identify the optimum adsorbent particle design and would enable to study
96 the effect of the adsorbent properties on the gas product purity. In terms of PSA model
97 validations, a study developed by Knox et al. [25] examined the accuracy of the parameter
98 estimation with data from breakthrough curves when using both the mass transfer and
99 dispersion coefficients as varying parameters, an approach used by several studies. The results
100 of the study suggested that axial dispersion should be measured inside the bed as the
101 experimental data can exhibit concentration front sharpening at the outlet of the bed. Then the
102 mass transfer coefficient can be obtained via parameter estimation.

103 In this work, a PSA model has been compared to experimental breakthrough curves obtained
104 from N₂ and CO₂ mixtures in a fixed-bed reactor, using TEPA-modified (AC-TEPA) and a
105 novel MEA-MDEA-modified (AC-MEA-MDEA) activated carbon granules. The modified

106 activated carbons were compared with the unmodified activated carbons (AC-unmodified) in
107 a flow process, based on their capacity and the breakthrough time of the experiments.

108 The mass transfer coefficient of the modified adsorbents was determined using a Maximum
109 Likelihood Parameter Estimation algorithm developed by PSE (Process Systems Enterprise),
110 which minimizes the standard deviation between the model results and the experimental data
111 using an optimization problem. The response of the experimental adsorption process was
112 recorded at the outlet of the bed, when the adsorbing component (CO₂) appeared. The level of
113 dispersion of the fixed-bed reactor and the surrounding system was previously determined from
114 experimental data using glass beads inside the reactor.

115 This work also presents the results of a sensitivity analysis for a range of adsorbent properties
116 and process variables using PSA. This enables to identify the variables to which the purity of
117 the carbon dioxide and hydrogen gas products are more sensitive, such that the process can be
118 optimized.

119 Previous work studied the effect of the type of adsorbent [26] and the adsorbent properties
120 [27,28] on the performance of the carbon dioxide capture. Some authors also studied the effect
121 of the PSA process variables, such as the number of pressure equalization steps and the feed
122 pressure, on the capture performance [27,29]. This work adds a number of adsorbent
123 parameters and process variables (particle diameter and bed length to diameter ratio), as well
124 as, a carbon dioxide rinse step to previously reported PSA sensitivity analysis studies.

125

126 **2. Materials and methods**

127 **2.1. Chemical impregnation procedure**

128 Activated Carbon Norit[®] RB1 was selected as a precursor in this work, due to the
129 demonstrated high adsorption capacity and selectivity towards carbon dioxide.

130 Impregnation via solvents was selected to improve the overall adsorption performance of the
131 activated carbons. This process adds an amount of chemical solution to the surface of the
132 adsorbent, following the methodology proposed by Khalil [30].

133 The AC-MEA-MDEA was prepared by modifying the activated carbon surface with a blend
134 between Monoethanolamine (MEA) and Monodiethanolamine (MDEA) solvents, with a
135 concentration of 0.4 and 0.6 (molar basis), respectively. An amount of 20 g activated carbon
136 sample was placed in a beaker for impregnation. The MEA-MDEA solution (150 ml) was
137 prepared by the addition of 45 ml of each solvent in 60 ml of deionized water. This solution
138 was magnetically stirred at 500 rpm for thirty seconds, aiming the complete solvent dissolution.
139 Then, the amine solution was added to the beaker containing the activated carbon. The molar
140 ratio between the amines and the activated carbon was 1:0.6 (mol AC:mol MEA-MDEA).

141 The beaker was then stirred at 500 rpm for one hour at room temperature to enhance the
142 chemical interaction between the solvent and the activated carbon surface. The excess of
143 solvent was removed from the beaker with a pipette, and then the adsorbent was transferred to
144 a crucible boat and dried in an oven at 150°C under nitrogen flow for 24 h.

145 The chemical treatment for the AC-TEPA (1:0.3, mol AC:mol TEPA) followed the same
146 order as the AC-MEA-MDEA. Instead, 150 ml of TEPA (90 ml of TEPA and 60 ml of
147 deionized water) solution was added to the activated carbons' surface. The activated carbons
148 were immersed in 150 ml of HCl 5M solution in a beaker and magnetically stirred at 500 rpm
149 for one hour. Deionized water was applied to remove the HCl excess in the activated carbons'
150 surface, and pH tapes were used to evaluate the neutralization of the material. Lastly, the
151 adsorbent was placed in the oven to dry for 24 hours at 150°C.

152

153 **2.2. Pressure Swing Adsorption (PSA) experimental studies with a fixed-bed reactor.**

154 The dynamic adsorption behavior of the ACs was studied in a fixed-bed reactor (stainless
155 steel; mass: 552.14 g; diameter: 2.5 cm; length: 6.9 cm; height: 2 cm), as shown in Figure 1.
156 Mass flow controllers (Brooks 5850 thermal mass; nitrogen maximum flow rate: 400 Nml.min⁻¹;
157 carbon dioxide maximum flow rate: 100 Nml.min⁻¹) (MFC, numbers 1 and 2) were used to
158 keep a constant gas flowrate to the inlet of the bed, from carbon dioxide and nitrogen cylinders
159 (both with purity of 99.99%) in the rig. Transducers (Swagelok S; pressure range: 0 – 42 bar)
160 (numbers 3 and 12) worked as pressure sensors, which displayed the inlet and outlet pressure
161 in a panel placed next to the rig.

162

Figure 1.

163 Numbers 4, 5 and 14 in Figure 1 show the bypass (Swagelok Stainless Steel Tee-Type
164 Particulate Filter, 1/4 in), which works as a gas flow pathway to the reactor or directly to the
165 exhaust (16). The adsorption temperature was monitored with two K-type thermocouples (7
166 and 9) placed in the inlet and outlet of the bed. A relief valve (Swagelok 316, pressure range:
167 24.1-51.7 bar) was used to secure safe operation and a back-pressure regulator (Swagelok 316
168 Stainless Steel PR Regulator, pressure range: 0 – 500 psig) (13) controlled the fixed-bed reactor
169 pressure.

170 A CO₂ analyzer (SERVOFLEX MINIMP 5200) (10) measured the carbon dioxide
171 concentration in the outlet of the reactor. Then the gas was directed to vent/exhaust (11). This
172 equipment was calibrated for a low range (0%) with pure nitrogen (200 Nml/min) and a high
173 range (100%) with pure carbon dioxide flow (100 Nml/min). The silica gel (dried at 140°C
174 overnight and then placed in the CO₂ analyzer inlet) was used as a drying agent, for the

175 accuracy of the CO₂ readings, as specified by the analyzer manufacturer. The placement of this
176 material did not interfere with the results reading.

177 The experimental adsorption tests with the ACs started by flowing pure nitrogen (200
178 Nml/min) into the bed (at 150°C and 1 bar, for 3600 s), to remove residual gas components
179 from the system. The mass of the solid in the bed was 10 g for all experiments. When the bed
180 was completely pressurized to 25 bar, the nitrogen flow rate was reduced to 120 Nml/min and
181 the carbon dioxide flow started (80 Nml/min) to begin the adsorption test. The experiments
182 were conducted with 30% and 40% CO₂ feed fractions. The adsorption experiments lasted 1 h.
183 The amount of carbon dioxide adsorbed per mass unit of the activated carbons (Q_{tCO_2}) was
184 determined from a mass balance (eq 1) applied to the bed during the adsorption experiments
185 and by integrating the area above the breakthrough curve.

$$186 \quad Q_{tCO_2} = \frac{1}{m_{ads}} \left[\int_0^t (F_{CO_2,in} - F_{CO_2,out}) dt - \frac{Y_{CO_2,feed} P V_b}{RT} \right] \quad (1)$$

187 where, $m_{adsorbent}$ corresponds to the mass of adsorbent in the fixed-bed reactor, $F_{CO_2,in}$ and
188 $F_{CO_2,out}$ are the molar flowrates of carbon dioxide at the inlet and outlet of the bed, respectively.
189 t_s is the time to achieve the saturation of the adsorbent, $Y_{CO_2,feed}$ is the molar fraction of carbon
190 dioxide in the feed stream. P and T are the pressure and temperature of the bed, V_b is the bed
191 volume and R is the universal gas constant.

192

193 **3. Theory**

194 The adsorption step of PSA was compared to a one-dimensional model that included 30%
195 CO₂ and 70% N₂, as well as, 40% CO₂ and 60% N₂ mol percentages in the feed at 25 bar and
196 ambient temperatures (25°C), the same as the laboratory conditions.

197 The main assumptions underlying the partial algebraic differential equations (PADEs) used
 198 in the PSA model were the following, supported by previous studies [15, 30–36]:

199 • The Soave-Redlich-Kwong equation of state was used to calculate the compressibility
 200 factor for this system, where the value was over 0.9. Therefore, flowing gases were considered
 201 ideal.

202 • There were no radial variations in pressure, temperature, and concentration of the
 203 components in the gas and solid phases.

204 • The solid and gas phases were in thermal equilibrium and the bulk density of the solid
 205 remains constant.

206 These assumptions were incorporated when developing the PADEs that define the evolution
 207 of the concentration of the components (overall and component mass balances) and
 208 temperature (energy balance) in the fixed-bed reactor.

209 The overall (eq 2) and component (eq 3) mass balance equations were developed including
 210 the accumulation, inlet and outlet, adsorption and dispersion terms of the reactor. The energy
 211 balance (eq 4) equation assumed the heat accumulation in the solid and the gas phase, heat
 212 transfer in the gas phase, the heat generated from adsorption and heat transfer from the gas
 213 phase to the reactor wall.

$$214 \quad \varepsilon_t \frac{\partial C(z)}{\partial t} = -\varepsilon_b \frac{\partial(C(z)v(z))}{\partial z} + \varepsilon_b D_x \frac{\partial^2 C(z)}{\partial z^2} - (1 - \varepsilon_b) \sum_{i=1}^{N_{comp}} \frac{\partial Q(i,z)}{\partial t} \quad (2)$$

$$215 \quad \varepsilon_t \frac{\partial Y(i,z)}{\partial t} = -\varepsilon_b v(z) \frac{\partial Y(i,z)}{\partial z} + \varepsilon_b D_x \left(\frac{\partial^2 Y(i,z)}{\partial z^2} + \frac{2}{C(z)} \frac{\partial Y(i,z)}{\partial z} \frac{\partial C(z)}{\partial z} \right) - \frac{(1-\varepsilon_b)}{C(z)} \left(\frac{\partial Q(i,z)}{\partial t} - \right.$$

$$216 \quad \left. Y(i,z) \sum_{i=1}^{N_{comp}} \frac{\partial Q(i,z)}{\partial t} \right) \quad (3)$$

$$\begin{aligned}
217 \quad & e c_{p,g(z)} \frac{\partial(T(z)v)}{\partial z} + \varepsilon_t e c_{p,g(z)} \frac{\partial T(z)}{\partial t} + \varepsilon_t e_s c_{p,s} \frac{\partial T(z)}{\partial t} - (1 - \varepsilon_b) e_s \sum_{i=1}^{N_{comp}} \Delta H_{ads(i)} \frac{\partial Q(i,z)}{\partial t} + \\
218 \quad & h_i(T(z) - T_{wall}) = \lambda \frac{\partial^2 T(z)}{\partial z^2} \quad (4)
\end{aligned}$$

219 The dispersion coefficient was determined comparing a dispersion model with the glass-
220 beads experiments, using parameter estimation. The fixed-bed reactor was filled with glass
221 beads of the same size of the activated carbons. The dispersion model included the inlet pipe
222 (ID= 1×10^{-3} m, L= 0.5 m), which connected the CO₂ and N₂ feed vessels with the fixed-bed
223 reactor and the outlet pipe (ID= 1×10^{-3} m, L= 0.1 m), which connected the reactor with the CO₂
224 analyzer. This system was isothermal as adsorption did not occur in the beads and the reactor
225 wall was isolated. Eq 5 shows the mass balance equation for the dispersion model for the
226 reactor filled with glass beads and the surrounding system.

$$227 \quad \frac{\partial Y(z)}{\partial t} = -v \frac{\partial(Y(i,z))}{\partial z} + D_x \frac{\partial^2 Y(i,z)}{\partial z^2} \quad (5)$$

228 The equilibrium between the gas phase and the activated carbons' surface was represented
229 by the Langmuir isotherm (eq 6), based on the equilibrium data obtained for the activated
230 carbons from the HPVA experiments (Appendix A, Figures A1 and A2). The Ergun equation
231 (eq 7) was used to calculate momentum losses [15,31,34,35].

232 The limiting step of mass transfer resistance is diffusion through micro-pores, represented
233 by the linear driving force (LDF) model (eq 8), which describes the adsorption kinetics [15,31–
234 33,36]. This assumption is supported by a previous study, where this simplification was shown
235 to be valid for PSA systems featuring activated carbons [35].

$$236 \quad Q_{(z)}^* = \frac{q_m b P(z) RT(z)}{1 + b P(z) RT(z)} \quad (6)$$

$$237 \quad \frac{\partial P(z)}{\partial z} = 150 u_{g(z)} \frac{(1-\varepsilon_b)^2}{D_p^2 \varepsilon_t^3} + 1.75 \frac{(1-\varepsilon_t)}{D_p \varepsilon_t^3} e v(z)/v(z)/ \quad (7)$$

238
$$\frac{\partial Q_{(i,z)}}{\partial t} = K_{(i)}(Q_{(i,z)}^* - Q_{(i,z)}) \quad (8)$$

239 The results of the model were obtained using gPROMS[®] ProcessBuilder 1.1.0. The custom
 240 model was developed in the gPROMS[®] language environment, where the model was divided
 241 into various subtasks: specification of parameters, variables, boundary conditions, and
 242 equations.

243 The thermodynamics of the process were calculated using the Multiflash[®] package. The
 244 backward finite difference method (BFDM) was used to discretize the component and overall
 245 concentrations, velocity, and temperature variables (against the flow, due to the diffusion
 246 phenomena). However, the pressure was discretized using the forward finite difference method
 247 (FFDM), as the pressure was specified in the outlet of the bed.

248 The boundary conditions of the model are shown in eqs 9–18. The inlet boundary conditions
 249 for the fraction of the components and temperature variables changed for each step of the PSA
 250 model, by introducing discontinuities that cause sudden changes in these variables. The outlet
 251 boundary condition of the pressure (P_{end}) was kept constant for the adsorption (25 bar), purge
 252 and rinse (1 bar) steps.

253
$$-\varepsilon_b D_x \frac{\partial C_i}{\partial z_{z=0}} = v_{z=0}(C_{i,feed} - C_{i,z=0}) \quad (9)$$

254
$$-\varepsilon_b \lambda \frac{\partial T}{\partial z_{z=0}} = v_{z=0} e c_{p,g,z=0} (T_{feed} - T_{z=0}) \quad (10)$$

255
$$v_{z=0} = v_{feed} \quad (11)$$

256
$$\frac{\partial C_i}{\partial z_{z=L}} = 0 \quad (12)$$

257
$$\frac{\partial T}{\partial z_{z=L}} = 0 \quad (13)$$

258
$$\frac{\partial v}{\partial z_{z=L}} = 0 \quad (14)$$

259
$$P_{z=L} = P_{end} \quad (15)$$

260 For the pressurization (press), pressure depressurization (depress), and pressure equalization
 261 (equal) steps, the outlet boundary condition of the pressure was described by a transition
 262 equation (eq 16–18), between the adsorption pressure (P_{ads}), equalization pressure (P_{eq}) and the
 263 atmospheric pressure (P_{atm}). The change was described by a linear equation that modelled a
 264 linear valve.

265
$$\frac{\partial P_{press}}{\partial t}_{z=L} = \left(\frac{P_{ads} - P_{atm}}{t_{pressurization}} \right) \quad (16)$$

266

267
$$\frac{\partial P_{depress}}{\partial t}_{z=L} = \left(- \frac{P_{eq} - P_{atm}}{t_{depressurization}} \right) \quad (17)$$

268

269
$$\frac{\partial P_{equal}}{\partial t}_{z=L} = \left(- \frac{P_{ads} - P_{eq}}{t_{equalization}} \right) \quad (18)$$

270 The parameters used in the model (adsorbent and bed properties) are shown in Table 1. The
 271 conditions are the same as those for the laboratory experiments. The Langmuir isotherm
 272 parameters and the heat of adsorption were determined from the HPVA data of the activated
 273 carbons. The axial heat dispersion coefficient and the effective heat transfer coefficient were
 274 calculated using the Wakao and Funazkri correlations [37–39]. Initially (at $t = 0$), it is assumed
 275 that there is only nitrogen at high pressures (25 bar) and ambient temperatures (25°C) in the
 276 fixed-bed, and no carbon dioxide on the surface of the adsorbent.

277 **Table 1.** Adsorbent and fixed-bed reactor parameters for the Pressure Swing Adsorption
 278 model.

Amine-modified ACs data		Fixed-bed reactor data	
Particle density, e_s (kg m^{-3})	262	Bed length, L (m)	0.069
Particle void fraction, ε_p	0.74	Bed void fraction, ε_b	0.48
Particle diameter, d_p (m)	0.001	Bed length/diameter ratio, L/D	2.76
Sorbent specific heat, cp_s ($\text{kJ kg}^{-1} \text{K}^{-1}$)	1	Wall specific heat, cp_w ($\text{kJ kg}^{-1} \text{K}^{-1}$)	0.46
Adsorption heat CO_2 , ΔH (kJ mol^{-1})	24.8	Wall thickness, L_w (m)	0.002
Adsorption heat N_2 , ΔH (kJ mol^{-1})	8.4	Wall density, e_w (kg m^{-3})	7700
Maximum monolayer coverage capacity for CO_2 , q_{m,CO_2} (mol kg^{-1})	9.2	Effective heat transfer coefficient, h_i ($\text{kW m}^{-2} \text{K}^{-1}$)	500
Langmuir equilibrium constant for CO_2 , b_{CO_2} (Pa^{-1})	3×10^{-6}	Axial heat dispersion coefficient, λ ($\text{W m}^{-1} \text{K}^{-1}$)	1.5

279

280

281 4. Results and discussion

282 4.1. Performance of the novel MEA-MDEA-modified ACs under PSA conditions.

283 The experimental breakthrough data from the adsorption step was generated using a binary
284 mixture of CO_2 and N_2 (40% and 60%, molar basis) at 25°C and 25 bar, using the AC-
285 Unmodified and the AC-MEA-MDEA in the fixed-bed reactor, one at a time.

286 Nitrogen was used instead of hydrogen to test the adsorption behavior of the adsorbents in
287 pre-combustion conditions, due to safety concerns and to the fact that the performance of the
288 CO_2 - H_2 mixture was expected to be far more efficient than that of CO_2 - N_2 mixture. This is due
289 to the light weight of the hydrogen gas compared to nitrogen. A study by Garcia et al. [40] on
290 AP3-60 activated carbons showed that the fraction of carbon dioxide captured for a CO_2 - N_2

291 mixture was ~0.82 of the total volume of gas captured, whereas it was ~0.92 for a CO₂-H₂
292 mixture.

293 The comparison between the two systems was quantified using previous studies, which
294 measured the adsorption capacity of the activated carbons for CO₂-N₂ and CO₂-H₂ systems. In
295 the studies that compared adsorbent capacities, the capacity of the activated carbons to adsorb
296 hydrogen varied between 0.04 and 0.06 mmol/g [35,38,41], whereas the capacity of the
297 activated carbons to adsorb carbon dioxide varied between 9 to 10 mmol/g. The adsorbed
298 carbon dioxide in the breakthrough experiments for this study was 9.6 mmol/g for the
299 unmodified activated carbon, whereas it was 10.6 mmol/g for the AC-MEA-MDEA. The
300 adsorbent capacity of nitrogen reported by Lopes et al. [39] was 0.14 mmol/g, which was
301 similar to the capacity of the activated carbons to adsorb hydrogen.

302 Figure 2 shows the breakthrough curves obtained for the experiments with the AC-MEA-
303 MDEA and the AC-Unmodified adsorbents at 25 bar. The total amount of carbon dioxide
304 adsorbed per mass unit of the adsorbent was calculated by integrating the area above the
305 breakthrough curve, following eq 1. The AC-MEA-MDEA adsorbed 10.6 mmol CO₂/g
306 adsorbent, whereas the AC-Unmodified adsorbed 9.6 mmol CO₂/g adsorbent.

307 **Figure 2.**

308 The amine modified activated carbons showed good results for post-combustion capture
309 conditions using 15% CO₂ and 85% H₂ feed conditions in previous studies [22]. These
310 adsorbents show far promising results for pre-combustion capture using 40% CO₂ and 60% N₂
311 mixtures, as shown in Figure 2.

312 Additionally, the AC-MEA-MDEA showed improved selectivity for carbon dioxide
313 compared to the AC-Unmodified. This was analyzed by measuring the amount of nitrogen

314 leaving the fixed-bed reactor during the experiments (Appendix B, Table B1). The amount of
315 nitrogen that left the bed during the adsorption experiment was 7625 mg with the AC-
316 Unmodified, whereas this amount was 8733.1 mg in the experiment using AC-MEA-MDEA.
317 From these values it was derived that the amount of pure nitrogen produced with the AC-MEA-
318 MDEA was 15% higher.

319 The later break-point (1274 s) for the experiment using AC-MEA-MDEA, compared to the
320 experiment with the AC-Unmodified (992 s), is mainly due to the improved capacity of the
321 amine-modified adsorbent compared to the precursor. The steeper breakthrough curve of the
322 AC-MEA-MDEA also shows an improved mass transfer between the gas and the solid surface.
323 This can be explained by the incorporation of the active amine sites in the porous surface of
324 the carbons [42–44] and supports the success of the novel surface modification.

325

326 **4.2. Model validation via parameter estimation and ACs mass transfer coefficient** 327 **determination.**

328 In order to ensure the accuracy of the parameter estimation between the model and the
329 activated carbons, the dispersion coefficient was firstly obtained by fitting a dispersed plug
330 flow model (eq 5) against experimental data using glass beads under CO₂-N₂ mixtures and PSA
331 experimental conditions.

332 Figure 3 shows the breakthrough curves for the plug-flow model and the experimental data
333 for the glass beads only, which enabled to predict the dispersion coefficient to be $5 \times 10^{-6} m^2 s^{-1}$.
334 The dispersion coefficient was then fixed at the value derived from the glass beads to enhance
335 the accuracy of the parameter estimation between the PSA model and the laboratory
336 experiments with the amine modified ACs [25]. The mass transfer coefficient was the
337 parameter estimated from this fit.

338

Figure 3.

339 Once the dispersion coefficient was determined, the mass transfer coefficients of, both, AC-
340 MEA-MDEA and AC-TEPA activated carbons were compared. Figure 4a and Figure 4b show
341 the breakthrough curves for the parameter estimation for each of the surface modified ACs,
342 using 40% and 30% CO₂ fractions in the feed gas.

343

Figure 4a.

344

Figure 4b.

345 A good visual fit was achieved between the experiments and the model for both of the
346 adsorbents, with a sum of squared residuals (SSR) of 0.1% (a) and 0.3% (b), which is under
347 the 10% of the acceptable percentage for engineering purposes using parameter estimation. The
348 PSA model predicted accurately the breakthrough curves for the experiments using 30% and
349 40% CO₂ feed fraction with AC-MEA-MDEA and, 30% feed fraction with the AC-TEPA. The
350 PSA model using 40% CO₂ feed fraction with AC-TEPA showed a steeper breakthrough curve
351 than the one showed by the experiment, due to the chemisorption effects that may have been
352 introduced with the amine groups in the activated carbon surface. The results for the mass
353 transfer coefficient of the AC-MEA-MDEA and the AC-TEPA were 0.046 s⁻¹ and 0.074 s⁻¹,
354 respectively, and they are in the range of previously reported values for PSA processes using
355 activated carbons [15].

356 Although the AC-TEPA showed a greater mass transfer value and, thus, a steeper
357 breakthrough curve, the AC-MEA-MDEA showed to have a later break-point with around 3 to
358 4 minutes difference for both CO₂ feed fractions, due to their high capacity as shown in the
359 previous chapter. This could be explained by the insertion of a two-amine group solution (MEA
360 and MDEA) into the pores, instead of the insertion of a one-amine group solution, as reported
361 in previous publications [17].

362

363 **4.3. Effect of the adsorbent properties on the overall purity of H₂ and CO₂**

364 After the model verification, a seven-step PSA model was developed which considered a
365 mixture of 40% carbon dioxide and 60% hydrogen entering the fixed-bed reactor. This process
366 simulated the conditions of a pre-combustion PSA process in an IGCC power plant. Table 2
367 shows the steps adopted in the model, which used Eqs 2-8 and Eqs 9-18 (boundary conditions)
368 to obtain the simulation results. Figure 5 shows the cycle sequence used in the PSA simulations.

369 **Table 2.** Conditions for the seven-step PSA model.

Steps	Description
Pressurization (P)	The fixed-bed is pressurized to 25 bar with a mixture of H ₂ and CO ₂
Adsorption (A)	Adsorption of CO ₂ in the surface of the adsorbent at 25 bar. Hydrogen is obtained as a product
Pressure equalization-depressurization (PE-D)	The bed pressure is decreased to 12.5 bar (the midpoint between the adsorption and the purge pressure) when connecting to a pressurizing bed
Depressurization (D)	The bed pressure is further decreased to 1 bar. The product gas goes to a purging bed.
Rinse (R)	CO ₂ enters the bed at 1 bar. CO ₂ is obtained as a product
Purge (Pu)	H ₂ enters the bed at 1 bar, coming from the depressurization step. CO ₂ is obtained as a product
Pressure equalization-pressurization (PE-P)	The bed pressure is increased to 12.5 bar (the midpoint between the purge and the adsorption pressure) when connecting to a depressurizing bed

370

371

Figure 5.

372 The process conditions used in the simulation were the same as those in the laboratory
 373 experiments at ambient temperatures and feed pressures for the pressurization and adsorption
 374 step, namely of 25 bar, and for the purge and the rinse step, namely 1 bar. Eq 19-20 were used
 375 to study the effect of the adsorbent properties on the overall purity of the carbon dioxide (Pu_{CO_2})
 376 and hydrogen (Pu_{H_2}) products. The adsorbent parameters were independently varied.

$$377 \quad Pu_{CO_2} = \frac{\int_{t=t_{rinse}}^{t=t_{purge}} C_{CO_2,z=L} v_{z=L} dt}{\sum_{i=1}^n \int_{t=t_{rinse}}^{t=t_{purge}} C_{i,z=L} v_{z=L} dt} \quad (19)$$

$$378 \quad Pu_{H_2} = \frac{\int_{t=0}^{t=t_{feed}} C_{H_2,z=L} v_{z=L} dt}{\sum_{i=1}^n \int_{t=0}^{t=t_{feed}} C_{i,z=L} v_{z=L} dt} \quad (20)$$

379 Firstly, the results of the mass transfer coefficient sensitivity analysis are illustrated in Figure
 380 6, which shows the evolution of the molar fraction of carbon dioxide at the end of the fixed-
 381 bed reactor for the seven-step pressure swing adsorption model. The break-point of the feed
 382 step does seem to be affected by variations in the mass transfer coefficient. With an increase
 383 from 0.02 s^{-1} to 0.1 s^{-1} in the mass transfer coefficient, the break-point occurs around two
 384 minutes later. The slope between the adsorption and, the purge and rinse steps remains constant,
 385 due to the depressurization of the bed before the break-point caused by the adsorbents'
 386 saturation. This step decreases the pressure in the bed and creates a pressure gradient between
 387 the inlet and the outlet of the bed. Carbon dioxide is not desorbed until the end of the bed
 388 reaches pressures of around 1 bar.

389 Secondly, the results for the rest of the adsorbent property values used in the sensitivity
 390 analysis are shown in Table 3, together with the carbon dioxide and hydrogen purity values
 391 obtained for each parameter value. The laboratory (default) values for those properties are
 392 shown with an asterisk in the table.

393 For the particle diameter (PD), the sensitivity analysis was simulated with a deviation of 25%
394 from the original size. Smaller particles may cause pressure drop issues. For the particle and
395 bed void fraction and for the mass transfer coefficient, the values were selected based on the
396 previous numbers shown for activated carbon adsorbents [23,24,44].

397 **Figure 6.**

398 Table 3 shows that the mass transfer coefficient is the variable that had the greatest effect on
399 the overall purities of CO₂. The purities of hydrogen did not deviate from 99% when changing
400 this variable. The values of the breakthrough capacity for carbon dioxide remain constant when
401 varying the mass transfer coefficient. The same was observed for the rest of the adsorbent
402 properties.

403 The most common correlation that has been used to calculate the mass transfer coefficient
404 is that shown by Farooq and Ruthven, which sums the micro-, meso- and macro-pore mass
405 transfer resistances [45]. This variable can also be calculated using the Peclet number
406 correlation [46]. These correlations have shown to be uncertain due to dispersion effects in the
407 bed [25]. In this study the mass transfer coefficient has been varied independently and the
408 results show that an adsorbent which shows a high mass transfer coefficient towards carbon
409 dioxide (of around 0.1 s⁻¹) enables to obtain a higher purity, of around 10%, in the final CO₂
410 product, compared to lower mass transfer coefficient values of around 0.04 s⁻¹. The mass
411 transfer coefficient affects the break-point (Figure 6) and, thus, the amount of carbon dioxide
412 adsorbed and the purity of the CO₂ product stream in the rinse and purge steps (between 1100
413 and 1700s).

414 **Table 3.** Calculated Purity (%) Values for the H₂ and CO₂ Products Streams for a Number of
415 Adsorbent Properties.

Particle diameter (m)	Purity H₂/CO₂ (%)	Particle void fraction (-)	Purity H₂/CO₂ (%)
0.75 × 10 ⁻³	99.5/82.1	0.55	99.4/82.7
1 × 10 ^{-3*}	99.4/81.9	0.74*	99.4/81.9
1.25 × 10 ⁻³	99.3/81.6	0.85	99.4/81.6
Bed void fraction (-)	Purity H₂/CO₂ (%)	MT coefficient (s⁻¹)	Purity H₂/CO₂ (%)
0.48*	99.4/81.9	0.02	99.2/71.9
0.6	99.4/81	0.04*	99.4/81.9
0.7	99.5/80.8	0.1	99.5/90.3

416

417 In terms of the particle and bed void fractions and the particle diameter, the purity of
418 hydrogen does not seem to be affected by those properties and remains constant at 99%, with
419 a marginal error of $\pm 0.1\%$. A plausible explanation for this is that if the adsorbent properties
420 are in an acceptable range for the adsorption of carbon dioxide, the outcome of hydrogen
421 product stream will be highly pure (over 99%), due to the lightness of the hydrogen gas and
422 the high affinity of the carbonaceous surface with the carbon dioxide gas for binary mixtures.

423 The purity of carbon dioxide gas is more sensitive to the properties of the adsorbent applied
424 in the given process conditions and is about 20%–30% lower than the purity of hydrogen, as
425 reported in most industrial processes where the light product (hydrogen) is the desired product
426 [35]. Decreasing the particle diameter favorably increases the purity of the CO₂ stream, due to
427 the greater external surface areas for adsorption in the fixed-bed reactor. It also favors the plug
428 flow in the bed, because the ratio of the bed to the particle diameter increases [25].

429 The recovery of the hydrogen and carbon dioxide products remained practically constant
430 varying the adsorbent properties. The recovery of carbon dioxide was around 52% for this
431 process, whereas it was around 75% for the hydrogen product. The recovery of these products
432 decreased, due to recycling hydrogen and carbon dioxide into the process, compared to
433 previous studies [27,29].

434

435 **4.4. Effect of the PSA process variables on the overall purity of H₂ and CO₂**

436 The sensitivity analysis for the seven-step PSA process variables (component feed fractions,
437 feed and purge pressures and reactor length to diameter ratio) was carried out the same way as
438 for the adsorbent properties, using eqs 2-20. The adsorbent properties in the model were set to
439 be the same as the AC-MEA-MDEA properties (Table 1) with a mass transfer coefficient value
440 of 0.046 s⁻¹.

441 The results for the process variables (feed pressure and feed component fractions) that had
442 the greatest effect on the breakthrough curves are illustrated in Figures 7-8. For the purpose of
443 consistency, one process variable value at a time was changed from the original laboratory
444 process. The process variable values used in the sensitivity analysis are shown in Table 4,
445 together with the carbon dioxide and hydrogen purity values obtained from the variable values.

446 The laboratory (default) values for those variables are shown with an asterisk in Table 4. The
447 rest of the values of Table 4 were selected based on previous conditions given in PSA process
448 studies [31–33,39]. The molar feed fraction of carbon dioxide was varied from 0.3 to 0.6 in
449 order to study the effect of the feed concentration of CO₂ in the adsorption step, with a view to
450 future work, to consider a carbon dioxide product recycle stream featuring a compressor.

451 Input purge pressures were decreased lower than atmospheric pressures (Table 4) in order to
452 investigate the need of a vacuum swing adsorption process. The reactor's length to diameter
453 ratios did not deviate more than 50% of the original value, due to design standards of process
454 engineering.

455 **Figure 7.**

456 **Figure 8.**

457 Figures 7 and 8 show that the selected process variables have a greater effect than the
 458 adsorbent properties on the overall CO₂ purities. On the one hand, the values of the
 459 breakthrough capacity remain constant, as do those of the adsorbent properties. On the other
 460 hand, the break-point of the feed step is greatly affected by variations in these variables.

461

462 **Table 4.** Calculated Purity (%) Values for the H₂ and CO₂ Products Stream for a Number of

463

PSA Process Variables.

Feed pressure (Pa)	Purity H ₂ /CO ₂ (%)	Purge pressure (Pa)	Purity H ₂ /CO ₂ (%)
15 × 10 ⁵	99.4/74.8	0.5 × 10 ⁵	99.4/96.4
20 × 10 ⁵	99.4/79.2	1 × 10 ^{5*}	99.4/81.9
25 × 10 ^{5*}	99.4/81.9	1.5 × 10 ⁵	99.4/77
CO ₂ feed fraction (-)	Purity H ₂ /CO ₂ (%)	Reactor length/ diameter ratio (-)	Purity H ₂ /CO ₂ (%)
0.3	99.3/73	2.5	99.5/84.7
0.4*	99.4/81.9	2.76*	99.4/81.9
0.6	99.5/91.6	3.5	99.1/79.5

464

465 The feed pressure (P_{feed}) affects only the overall purity of the carbon dioxide at high
 466 pressures (>15 bar). This can be due to the increase of the pressure ratio between the adsorption
 467 and purge step, which increases the CO₂ partial pressure in the pressure equalization and
 468 depressurization step. Although the purity of hydrogen is not affected, an increase of 5 bar in
 469 the feed pressure delays the break-point by 2 minutes (Figure 7). This explains why the overall
 470 purity of carbon dioxide is higher in the purge step. The total uptake of CO₂ increases due to a
 471 longer adsorption time, considering all PSA processes have the same duration.

472 The purge pressure has a greater effect than the feed pressure on the total purity of carbon
 473 dioxide as shown in Table 4. This is because the larger trade-off between the adsorption and
 474 the purge pressure when the last variable decreases to vacuum values and CO₂ is obtained as a
 475 product in the purge and rinse steps. The increase in the pressure gradient causes higher

476 depressurization rates, which enables a purer CO₂ stream of about 96.4% at vacuum pressures
477 of 0.5 bar. At this stage, a cost analysis should be estimated, to see whether it is worth including
478 a vacuum generator in the process.

479 The feed fraction of carbon dioxide in the adsorption step (Y_{feed}) has a greater effect on the
480 break-point than do both the purge and the feed pressures, as shown in Figure 8. With an
481 increase of about 20% in the feed fraction, the purity of carbon dioxide increases around 10%.
482 This enhances the mass transfer between the gas and the carbonaceous surface. At this stage,
483 it may be useful to introduce a recycle stream from the depressurization to the adsorption step,
484 which would increase the carbon dioxide partial pressure in the inlet of the reactor, supported
485 by most of the studies [31–33]. This would require a compressor in the recycle stream.

486 In terms of the reactor design, smaller length to diameter ratios yielded a higher purity of
487 carbon dioxide product (Table 4). When the ratio is about 10% smaller than that of the standard
488 laboratory reactor, the purity of carbon dioxide is 3% higher. A plausible explanation for this
489 could be the decreasing carbon dioxide partial pressure as the feed gas goes through the reactor,
490 which decreases the mass transfer driving force between the gas and the solid surface. Greater
491 diameters would enable higher adsorbent densities in the inlet of the bed, increasing the
492 adsorption capacity of the fixed-bed reactor in the inlet, where the carbon dioxide concentration
493 is at feed concentrations.

494 Deviant values on PSA process variables had a greater effect on the final purity of carbon
495 dioxide than did values of the adsorbent properties. The results showed that the process could
496 be scaled up using the parameters for amine-modified activated carbons and by including a
497 measure for the uncertainty of the adsorbent properties. These properties could cause a
498 maximum deviation of $\pm 10\%$ in the CO₂ product purity.

499 The PSA process variables, specifically, the feed fractions, the purge and feed pressures
500 seem to have a greater effect on the final CO₂ purity, with deviations of ± 10 to 20% in the
501 final purity values. Carbon dioxide concentrations of around 60% at 25 bar are preferred in the
502 feed during the adsorption step and 0.5 bar pressures in the purge and rinse steps.

503 The overall recovery of the hydrogen and carbon dioxide products was less sensitive
504 compared to the purity of these products, by varying these process conditions. The recovery
505 values obtained with the standard case (conditions shown with an asterisk in Table 4), were
506 52% and 75% for carbon dioxide and the hydrogen, respectively. These recovery values
507 deviated no more than 2% by varying the process conditions, because the amount of the
508 component products used in each step was not varied.

509 This sensitivity analysis shows that over 90% pure carbon dioxide cannot be obtained in the
510 basic case, but by varying the PSA process conditions, such as introducing a vacuum generator
511 to reach purge pressures of 0.5 bar or recycling carbon dioxide into the feed, purities of about
512 95% would be achieved. These results could be relevant and tested further at a larger scale. In
513 this case, the inclusion of a compressor or a vacuum generator would lead to a significant
514 increase of the energy penalty and the advantages in terms of separation performance would
515 thus need to be weighed against the disadvantage in terms of the energy efficiency of the
516 process.

517

518 **5. Conclusions**

519 A laboratory scale adsorption step under pre-combustion PSA conditions for IGCC power
520 plants was compared to a PSA model, using AC-TEPA and the novel AC-MEA-MDEA
521 modified activated carbons. The AC-MEA-MDEA adsorbents showed promising results

522 compared to the unmodified commercial Activated Carbon Norit[®], in terms of the carbon
523 dioxide adsorbed (of around 10% higher) and selectivity during the adsorption experiments in
524 a fixed-bed reactor.

525 A parameter estimation between an experimental adsorption step using AC-TEPA and AC-
526 MEA-MDEA adsorbents and a PSA model, showed a good fit between the breakthrough
527 curves, with an SSR less than 10%. Although the AC-TEPA showed a greater mass transfer
528 coefficient (0.074 s^{-1}), the delayed break-point (of around 200 s) of the AC-MEA-MDEA
529 adsorbents, makes them more promising for pre-combustion PSA.

530 A sensitivity analysis of the effect of the adsorbent properties showed that these variables
531 had a greater effect on the purity of carbon dioxide than on the purity of the hydrogen in the
532 product stream. The properties of the amine-modified adsorbents are important for obtaining
533 highly purified products (99.4% for hydrogen and 81.9% for carbon dioxide), specifically for
534 the purity of the light product stream.

535 A sensitivity analysis of the process variables of PSA showed that modifications in these
536 variables could yield to higher purities of CO₂ product stream (over 90%). Sensitivity analyses
537 showed that purities of carbon dioxide and hydrogen, as high as 91.6% and 96.4%, respectively,
538 could be achieved by increasing the carbon dioxide feed fraction by 50% and decreasing the
539 purge pressure by 50%. For these cases, the additional capital and operational costs should be
540 investigated, as there would be a need for a compressor for the recycle stream and a vacuum
541 generator to obtain pressures under atmospheric conditions. The recovery of these products did
542 not seem greatly affected by variations of the adsorbent properties and process variables, with
543 a maximum of 2% deviation varying the PSA process variables.

544

545 **Acknowledgements**

546 This work was supported financially by the Brazilian National Council for Scientific and
547 Technological Development (CNPq) from the program Science Without Borders (SwB,
548 206095/2014-7), as well as, the EPSRC and the Centre for Doctoral Training of Carbon
549 Capture and Storage and Cleaner Fossil Energy (EP/L016362/1). gPROMS[®] ProcessBuilder
550 software was provided in-kind by Process Systems Enterprise. Experimental data are available
551 at epapers.bham.ac.uk

552

553 **Supplementary data file: Appendix A and B**

554 Supplementary data of this article can be found online.

References

- [1] Global CCS Institute. Paris climate change targets cannot be met without CCS: COP23. vol. 30. Bonn, Germany.: 2017.
- [2] Edenhofer O, Pichs-Madruga R, Sokona Y, Farahani E, Kadner S, Seyboth K, et al. Mitigation of Climate Change. 2014. doi:10.1017/CBO9781107415416.
- [3] U.S. Energy Information Administration (EIA). International Energy Outlook 2016. vol. 0484(2016). Washington, DC: Office of Energy Analysis; 2016.
- [4] DOE/NETL. Advanced Carbon Dioxide Capture R&D Program: Technology Update. Pittsburgh, PA: 2013.
- [5] Wheeler D, Ummel K. Calculating CARMA: Global Estimation of CO₂ Emissions from the Power Sector. 2008.
- [6] Ummel K. Carma Revisited: An Updated Database of Carbon Dioxide Emissions from Power Plants Worldwide. SSRN Electron J 2012:2226505. doi:10.2139/ssrn.2226505.
- [7] Aaron D, Tsouris C. Separation of CO₂ from flue gas: A review. Sep Sci Technol 2005;40:321–48. doi:10.1081/SS-200042244.
- [8] Kohl AL, Nielsen RB. Gas Purification. vol. 10. 5th ed. Houston, TX. USA: Gulf Professional Publishing; 1997. doi:10.1016/B978-088415220-0/50009-4.
- [9] Campbell JM. Gas conditioning and processing. 4th ed. Norman, Okla.: Campbell Petroleum Series; 1998.
- [10] Cormos CC. Evaluation of reactive absorption and adsorption systems for post-combustion CO₂ capture applied to iron and steel industry. Appl Therm Eng 2016;105:56–64. doi:10.1016/j.applthermaleng.2016.05.149.

- [11] Ebner AD, Ritter JA. State-of-the-art adsorption and membrane separation processes for carbon dioxide production from carbon dioxide emitting industries. vol. 44. 2009. doi:10.1080/01496390902733314.
- [12] Gray ML, Soong Y, Champagne KJ, Pennline H, Baltrus JP, Stevens RW, et al. Improved immobilized carbon dioxide capture sorbents. *Fuel Process Technol* 2005;86:1449–55. doi:10.1016/j.fuproc.2005.01.005.
- [13] Houshmand A, Shafeeyan MS, Arami-Niya A, Daud WMAW. Anchoring a halogenated amine on the surface of a microporous activated carbon for carbon dioxide capture. *J Taiwan Inst Chem Eng* 2013;44:774–9. doi:10.1016/j.jtice.2013.01.014.
- [14] Liu H, Liu B, Lin LC, Chen G, Wu Y, Wang J, et al. A hybrid absorption-adsorption method to efficiently capture carbon. *Nat Commun* 2014;5:1–7. doi:10.1038/ncomms6147.
- [15] Agarwal A, Biegler LT, Zitney SE. Superstructure-Based Optimal Synthesis of Pressure Swing Adsorption Cycles for Precombustion CO₂ Capture. *Ind Eng Chem Res* 2010;49:5066–79. doi:10.1021/ie900873j.
- [16] Jansen D, Gazzani M, Manzolini G, Dijk E Van, Carbo M. Pre-combustion CO₂ capture. *Int J Greenh Gas Control* 2015;40:167–87. doi:10.1016/j.ijggc.2015.05.028.
- [17] Abanades JC, Wiley DE, Mangano E, Li H, Ho MT, Mattisson T, et al. Emerging CO₂ capture systems. *Int J Greenh Gas Control* 2015;40:126–66. doi:10.1016/j.ijggc.2015.04.018.
- [18] Grande CA. Advances in Pressure Swing Adsorption for Gas Separation. *ISRN Chem Eng* 2012;2012:1–13. doi:10.5402/2012/982934.
- [19] Hao G-P, Li W-C, Lu A-H. Novel porous solids for carbon dioxide capture. *J Mater*

- Chem 2011;21:6447. doi:10.1039/c0jm03564e.
- [20] Di Biase E, Sarkisov L. Molecular simulation of multi-component adsorption processes related to carbon capture in a high surface area, disordered activated carbon. *Carbon N Y* 2015;94:27–40. doi:10.1016/j.carbon.2015.06.056.
- [21] Jordá-Beneyto M, Suárez-García F, Lozano-Castelló D, Cazorla-Amorós D, Linares-Solano A. Hydrogen storage on chemically activated carbons and carbon nanomaterials at high pressures. *Carbon N Y* 2007;45:293–303. doi:10.1016/j.carbon.2006.09.022.
- [22] Samanta A, Zhao A, Shimizu GKH, Sarkar P, Gupta R. Post-Combustion CO₂ Capture Using Solid Sorbents: A Review. *Ind Eng Chem Res* 2012;51:1438–63. doi:10.1021/ie200686q.
- [23] Shafeeyan MS, Houshmand A, Arami-Niya A, Razaghizadeh H, Daud WMAW. Modification of Activated Carbon Using Nitration Followed by Reduction for Carbon Dioxide Capture. *Bull Korean Chem Soc* 2015;36:533–8. doi:10.1002/bkcs.10100.
- [24] Zhu B, Li K, Liu J, Liu H, Sun C, Snape CE, et al. Nitrogen-enriched and hierarchically porous carbon macro-spheres-ideal for large-scale CO₂ capture. *J Mater Chem A* 2014;2:5481–9. doi:10.1039/c4ta00438h.
- [25] Knox JC, Ebner AD, Levan MD, Coker RF, Ritter JA. Limitations of Breakthrough Curve Analysis in Fixed-Bed Adsorption. *Ind Eng Chem Res* 2016. doi:10.1021/acs.iecr.6b00516.
- [26] Casas N, Schell J, Blom R, Mazzotti M. MOF and UiO-67/MCM-41 adsorbents for pre-combustion CO₂ capture by PSA: Breakthrough experiments and process design. *Sep Purif Technol* 2013;112:34–48. doi:10.1016/j.seppur.2013.03.042.
- [27] Riboldi L, Bolland O. Comprehensive analysis on the performance of an IGCC plant

- with a PSA process integrated for CO₂ capture. *Int J Greenh Gas Control* 2015;43:57–69. doi:10.1016/j.ijggc.2015.10.006.
- [28] Khurana M, Farooq S. Integrated Adsorbent-Process Optimization for Carbon Capture and Concentration Using Vacuum Swing Adsorption Cycles. *AIChE J* 2017;63:2987–95. doi:10.1002/aic.15602.
- [29] Casas N, Schell J, Joss L, Mazzotti M. A parametric study of a PSA process for pre-combustion CO₂ capture. *Sep Purif Technol* 2013;104:183–92. doi:10.1016/j.seppur.2012.11.018.
- [30] Khalil SH, Aroua MK, Daud WMAW. Study on the improvement of the capacity of amine-impregnated commercial activated carbon beds for CO₂ adsorbing. *Chem Eng J* 2012;183:15–20. doi:10.1016/j.cej.2011.12.011.
- [31] Casas N, Schell J, Pini R, Mazzotti M. Fixed bed adsorption of CO₂/H₂ mixtures on activated carbon: Experiments and modeling. *Adsorption* 2012;18:143–61. doi:10.1007/s10450-012-9389-z.
- [32] Riboldi L, Bolland O, Ngoy JM, Wagner N. Full-plant analysis of a PSA CO₂ capture unit integrated in coal-fired power plants: Post- And pre-combustion scenarios. *Energy Procedia* 2014;63:2289–304. doi:10.1016/j.egypro.2014.11.248.
- [33] Riboldi L, Bolland O. Evaluating Pressure Swing Adsorption as a CO₂ separation technique in coal-fired power plants. *Int J Greenh Gas Control* 2015;39:1–16. doi:10.1016/j.ijggc.2015.02.001.
- [34] Dowling AW, Vetukuri SRR, Biegler LT. Large-Scale Optimization Strategies for Pressure Swing Adsorption Cycle Synthesis. *AIChE J* 2012;58:3777–91. doi:10.1002/aic.13928.

- [35] Ribeiro AM, Grande CA, Lopes FVS, Loureiro JM, Rodrigues AE. A parametric study of layered bed PSA for hydrogen purification. *Chem Eng Sci* 2008;63:5258–73. doi:10.1016/j.ces.2008.07.017.
- [36] Wang Y, Dowling AW, Krieff C, Walther A, Biegler LT. Pressure Swing Adsorption Optimization Strategies for CO₂ Capture. vol. 36. Elsevier; 2015. doi:10.1016/B978-0-444-63472-6.00008-2.
- [37] Wakao N, Kaguei S, Funazkri T. Effect of Fluid Dispersion Coefficients Particle-to-Fluid Heat Transfer Coefficients in Packed Beds. *Chem Eng Sci* 1979;34:325–36. doi:0009-2509/79/0301-0325/S02 00/0.
- [38] Lopes FVS, Grande CA, Ribeiro AM, Oliveira ELG, Loureiro M. Enhancing Capacity of Activated Carbons for Hydrogen Purification. *Ind Eng Chem Res* 2009;48:3978–90. doi:10.1021/ie801132t.
- [39] Lopes FVS, Grande CA, Rodrigues AE. Activated carbon for hydrogen purification by pressure swing adsorption: Multicomponent breakthrough curves and PSA performance. *Chem Eng Sci* 2011;66:303–17. doi:10.1016/j.ces.2010.10.034.
- [40] García S, Pis JJ, Rubiera F, Pevida C. Predicting mixed-gas adsorption equilibria on activated carbon for precombustion CO₂ capture. *Langmuir* 2013;29:6042–52. doi:10.1021/la4004998.
- [41] Hao P, Shi Y, Li S, Zhu X, Cai N. Correlations between adsorbent characteristics and the performance of pressure swing adsorption separation process. *Fuel* 2018;230:9–17. doi:10.1016/j.fuel.2018.05.030.
- [42] Bai BC, Kim EA, Lee CW, Lee Y-S, Im JS. Effects of surface chemical properties of activated carbon fibers modified by liquid oxidation for CO₂ adsorption. *Appl Surf Sci*

- 2015;353:158–64. doi:10.1016/j.apsusc.2015.06.046.
- [43] Campbell IM. *Catalysis at surfaces*. 1st Ed. London, UK: Chapman and Hall Ltd; 1988.
- [44] Sun N, Sun C, Liu J, Liu H, Snape CE, Li K, et al. Surface-modified spherical activated carbon materials for pre-combustion carbon dioxide capture. *RSC Adv* 2015;5:33681–90. doi:10.1039/C5RA02665B.
- [45] Farooq S, Ruthven DM. Heat effects in adsorption column dynamics. 2. Experimental validation of the one-dimensional model. *Ind Eng Chem Res* 1990;29:1084–90. doi:10.1021/ie00102a020.
- [46] Wang Y, Dowling AW, Krieff C, Walther A, Biegler LT. Pressure Swing Adsorption Optimization Strategies for CO₂ Capture. *Comput Aided Chem Eng* 2015;36:197–223. doi:10.1016/B978-0-444-63472-6.00008-2.

List of Figure Captions.

Figure 1. Schematic figure of the fixed-bed reactor process using Pressure Swing Adsorption (PSA) at laboratory scale.

Figure 2. Experimental breakthrough curves for the adsorption step of PSA using AC-Unmodified and AC-MEA-MDEA.

Figure 3. Comparison of the dispersed plug flow model against experimental data using glass beads under PSA conditions.

Figure 4a. Parameter estimation between the model and the experimental data for 30% and 40% CO₂ feed fractions using AC-MEA-MDEA.

Figure 4b. Parameter estimation between the model and the experimental data for 30% and 40% CO₂ feed fractions using AC-TEPA.

Figure 5. Schematic figure of the steps undertaken in the PSA process.

Figure 6. The effect of the mass transfer coefficient (K) on the outlet molar fractions of CO₂ for a seven-step PSA process.

Figure 7. The effect of feed pressure (P_{feed}) on the outlet molar fractions of CO₂ for a seven-step PSA process.

Figure 8. The effect of feed molar fractions (Y_{feed}) on the outlet molar fractions of CO₂ for a seven-step PSA process.

Figure 1

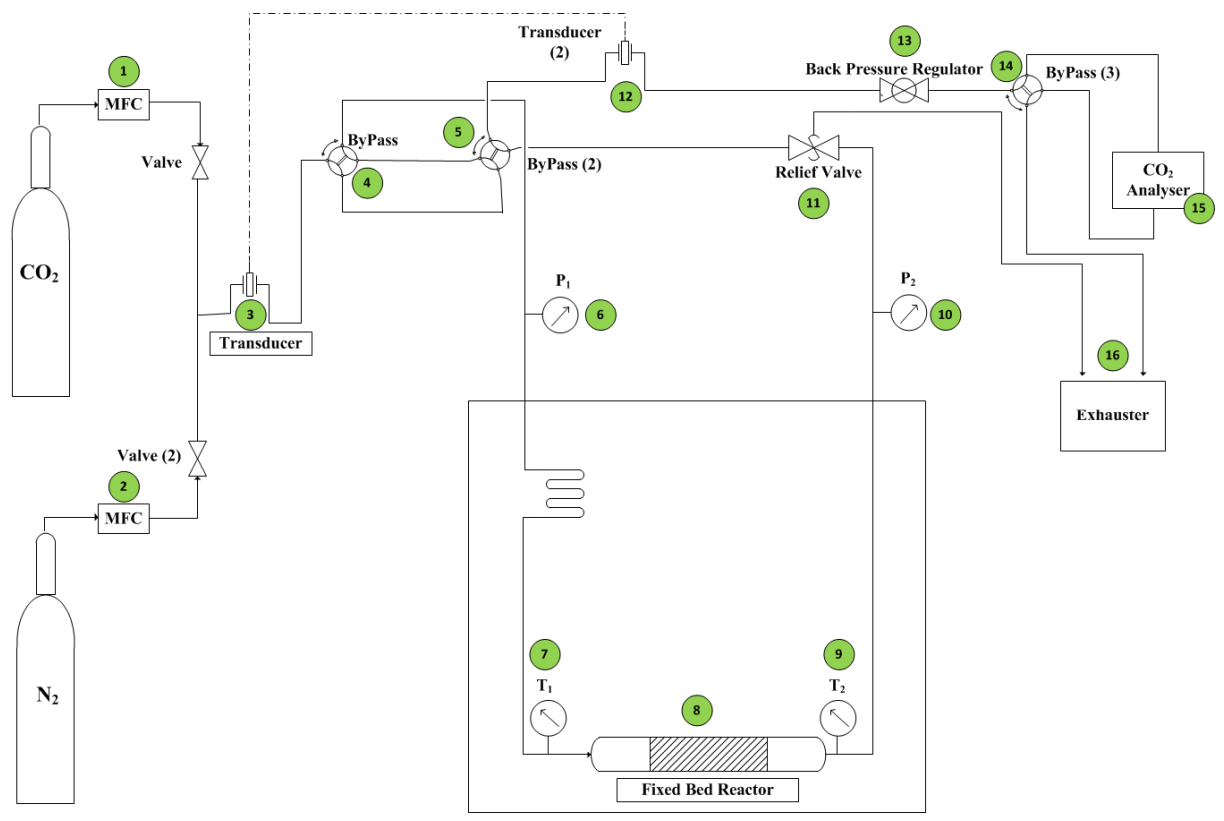


Figure 2

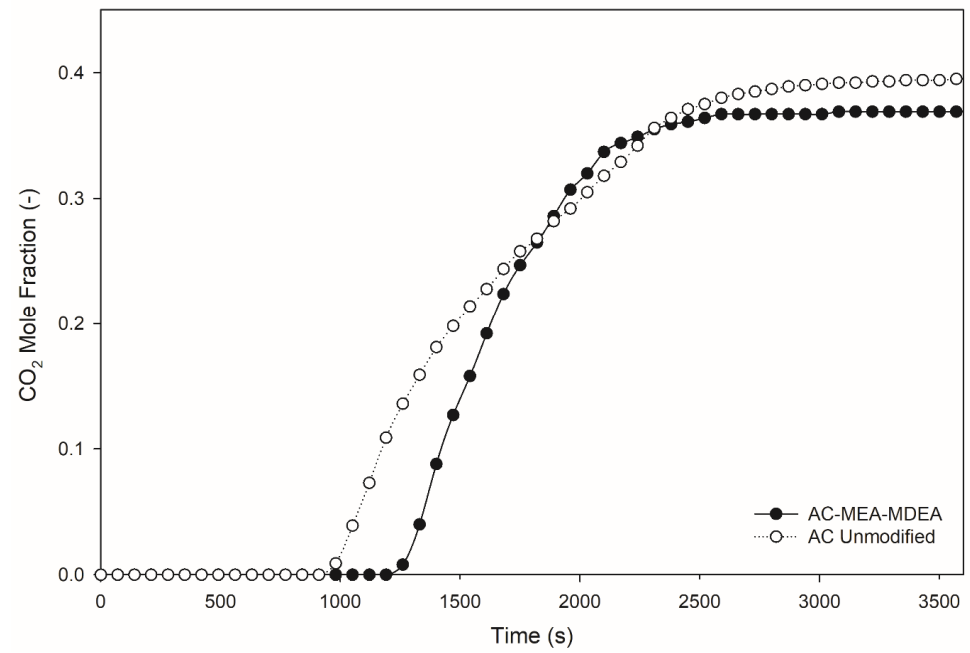


Figure 3

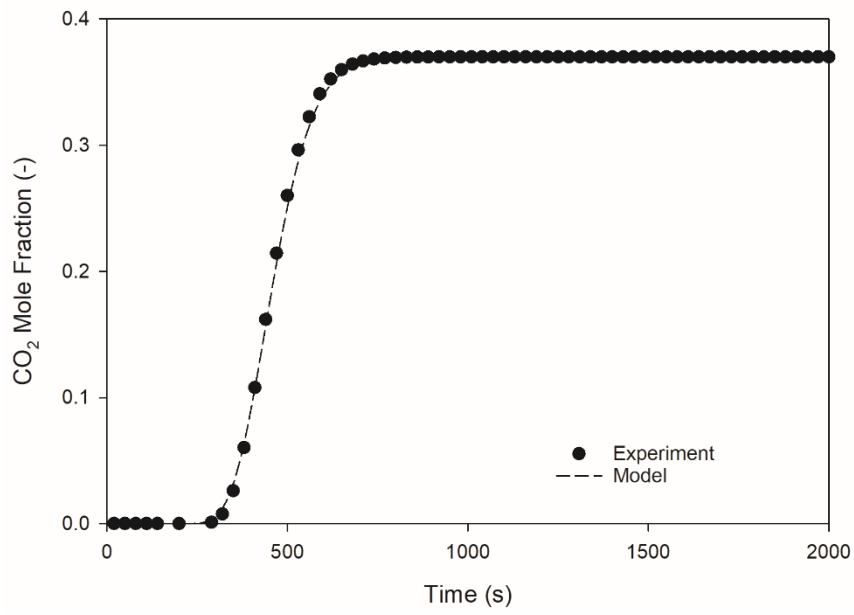


Figure 4a

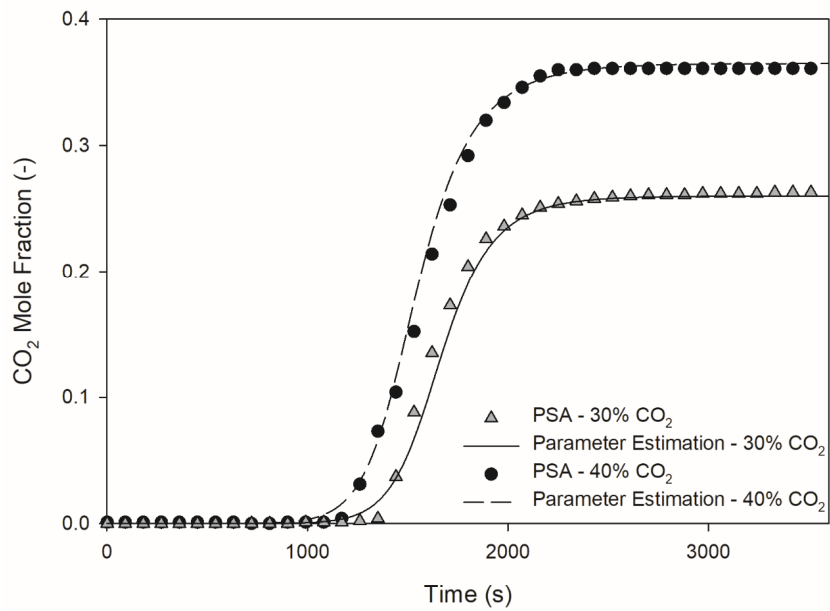


Figure 4b

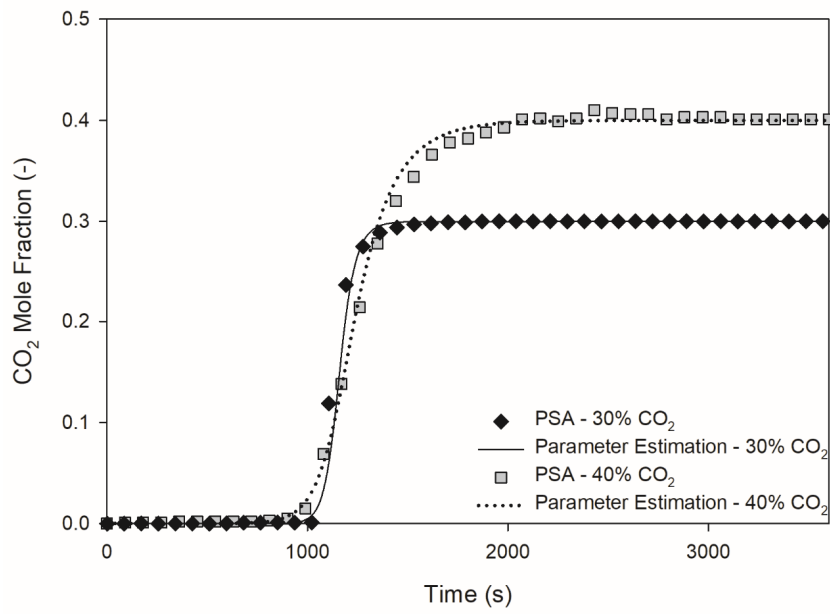


Figure 5

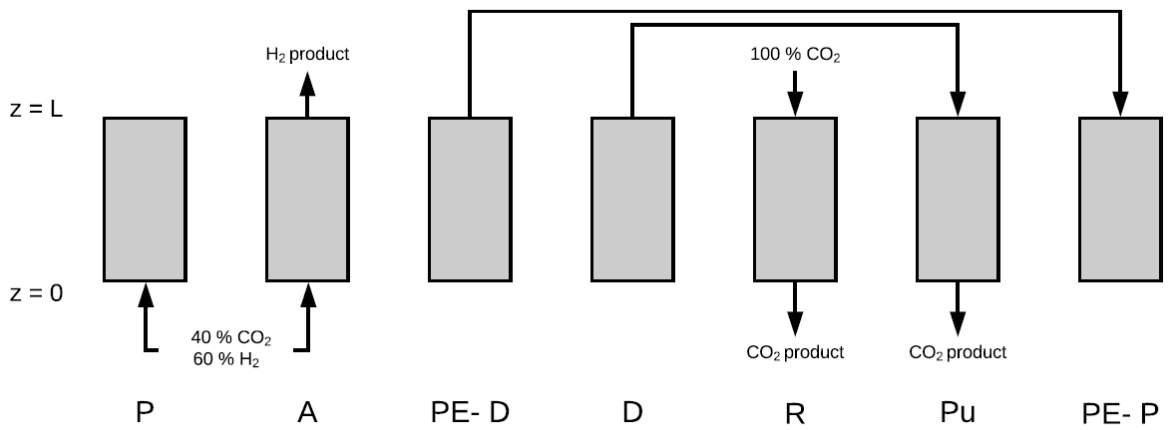


Figure 6

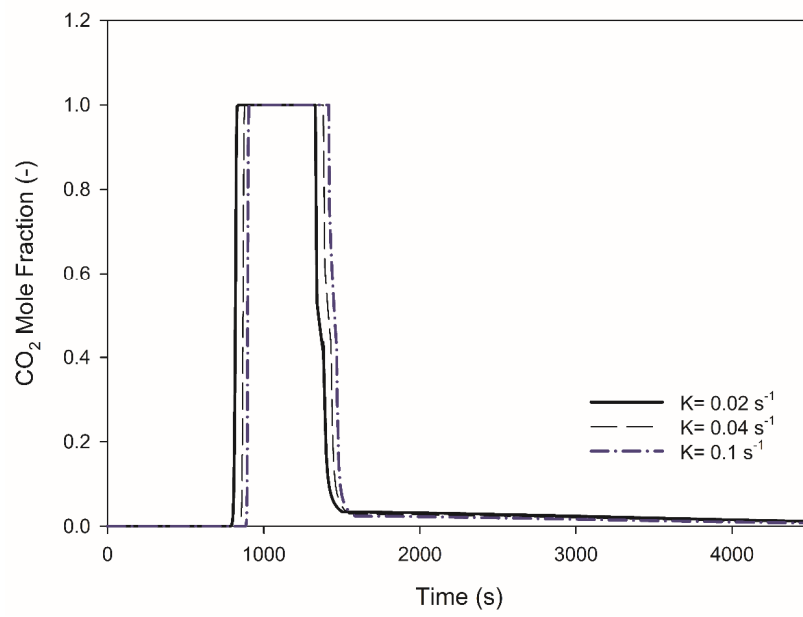


Figure 7

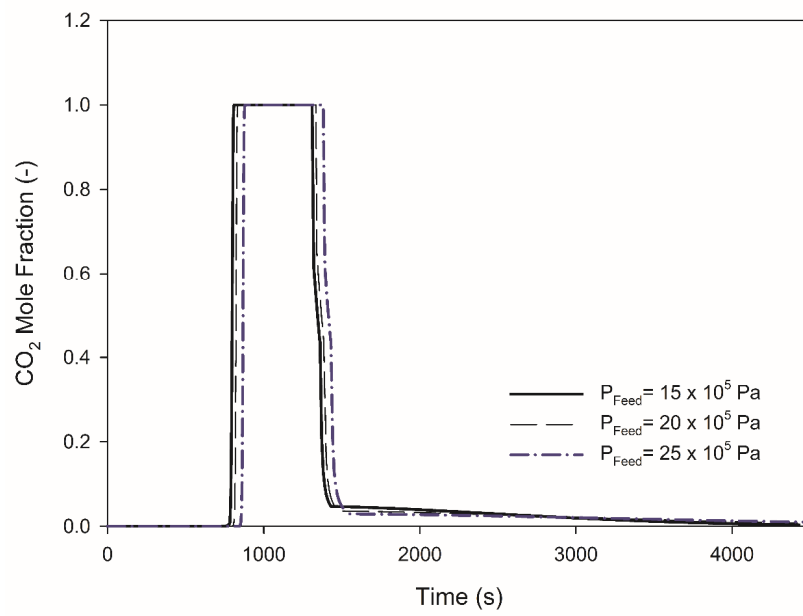


Figure 8

